Electronic Conduction in Freestanding Silicon Nanocrystal Films

Jingyang Zheng

Undergraduate Honors Thesis
University of Minnesota

Submitted under the supervision of Prof. James Kakalios to the University Honors Program at the University of Minnesota, Twin Cities in partial fulfillment of the requirements for the degree of Bachelor of Science, *summa cum laude*, in Physics.

May 13, 2017

Abstract

The dark conductivity of a 5.5 nanometer diameter freestanding silicon nanocrystal film was measured over a temperature range of 305K to 500K for increasing oxidation time. Comparisons are made to previous measurements of 12 nm films of similar composition. A stretched exponential time dependence for the decrease of the conductivity with air exposure time is observed for conductivity at 340K, while previous data indicated exponential decay or power law decay. Changes in conduction mechanism are also observed using the Zabrodskii analysis, indicating that conduction is either not thermally activated or that initial conductivity is temperature dependent.

Introduction

Nanocrystalline silicon (nc-Si) consists of small, roughly spherical particles of crystalline silicon with diameters of about 2-20 nm. They have many unique properties, including efficient and wavelength tunable light emission, multiple exciton generation, and various other optical properties.

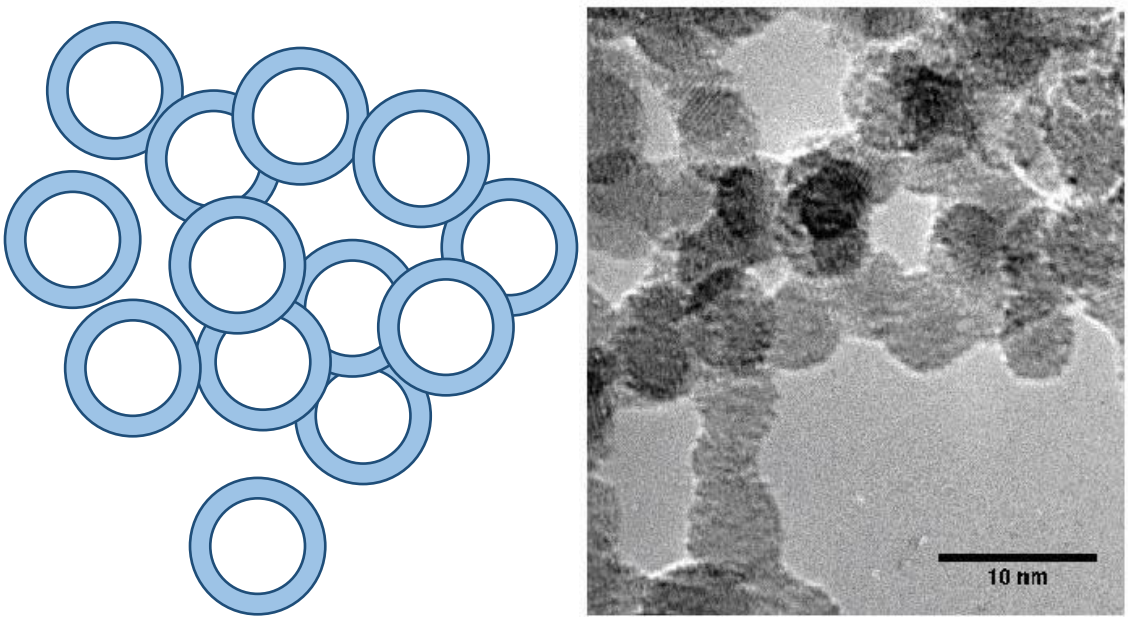

Figure 1. Diagram of nanocrystalline silicon with possible amorphous shell (left). Transmission Electron Microscope image (right, courtesy Brendon Jones).

When excited by UV light, a solution of nc-Si can emit light at different wavelengths depending solely on the size of the nanocrystal, with no chemical changes or doping required (as seen in Fig. 2). This could lead to various applications in systems where the introduction of other elements could adversely affect a compound.

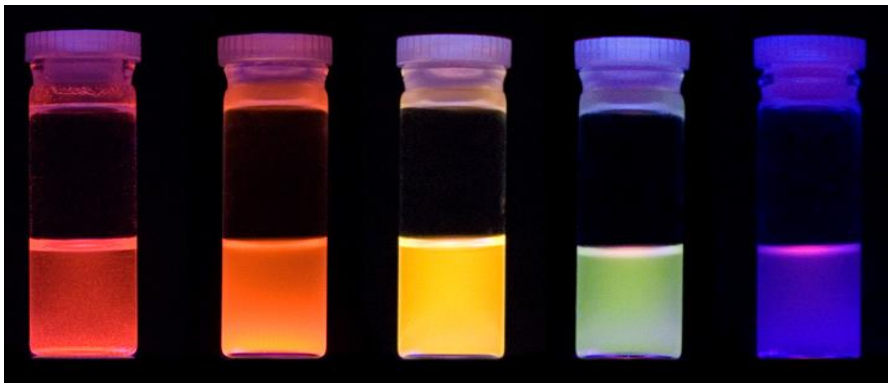

Figure 2 Emission of light from silicon nanocrystals in solution. Excitation by UV light. Seen in decreasing size order from left (20nm diameter) to right. Figure courtesy Prof. Kakalios.

Nanocrystalline silicon also has a wide range of applications in the development of thermoelectric materials, light emission from thin films, as well as cheap optoelectronic devices and novel devices utilizing quantum confinement [1,2]. It has use in photovoltaics as a cheaper and less breakable alternative to crystalline silicon in solar cells, as well as an alternative to amorphous silicon, which suffers from degradation by light exposure. Freestanding films of nc-Si are inexpensive, and can be fabricated by a wide range of techniques, including solid-gas reaction, liquid synthesis, laser pyrolysis of silane, laser ablation, laser vaporization-controlled condensation, and plasma assisted decomposition of silane [1]. These methods allow for tight control of the nanocrystal characteristics.

However, electronic transport in nc-Si has not been studied in as much detail as optical effects. The conductivity mechanism of nanocrystalline silicon is not well understood, and can be affected by various factors, including the thickness of the amorphous shell, the total diameter of the crystals, the surface to area ratio, the crystallinity, and the thickness of the film. These effects suggest that nc-Si may have controllable electronic properties. This work aims to study the effect of oxidation on the conductivity and conduction mechanism of a freestanding nc-Si film.

Theory and Background

Conductivity is defined as $\sigma = G \times g$ where the conductance $G = \frac{i}{V}\Omega^{-1}$is measured in our setup using a 50V potential. Here the geometry factor is determined by the thickness of the film, the width between the measurement electrodes, and the length of electrode used, giving $g = \frac{l}{w \times t} cm^{-1}$.

The temperature dependence of conductivity in silicon is modeled as

$$\sigma = \sigma_0 e^{-\frac{E_a}{kT}} \tag{1}$$

where the activation energy E_a is approximately half of the band gap and k is Boltzmann's constant. Here, $E_a = E_C - E_F$, the energy of the conduction band and the Fermi energy, respectively. At zero temperature, normal conduction cannot occur in a semiconductor because all of the filled Fermi states exist below the conduction band. The activation energy represents the energy required to bridge that gap and provide mobile charge carriers.

The thermally activated conductivity is described by a straight line on an Arrhenius plot, seen below for crystalline (Fig. 3) and amorphous silicon (Fig. 4), respectively. The slope in this plot is $-E_a$. In crystalline silicon (Fig. 3), deviations from linearity at low conductivity are caused by impurities in the sample.

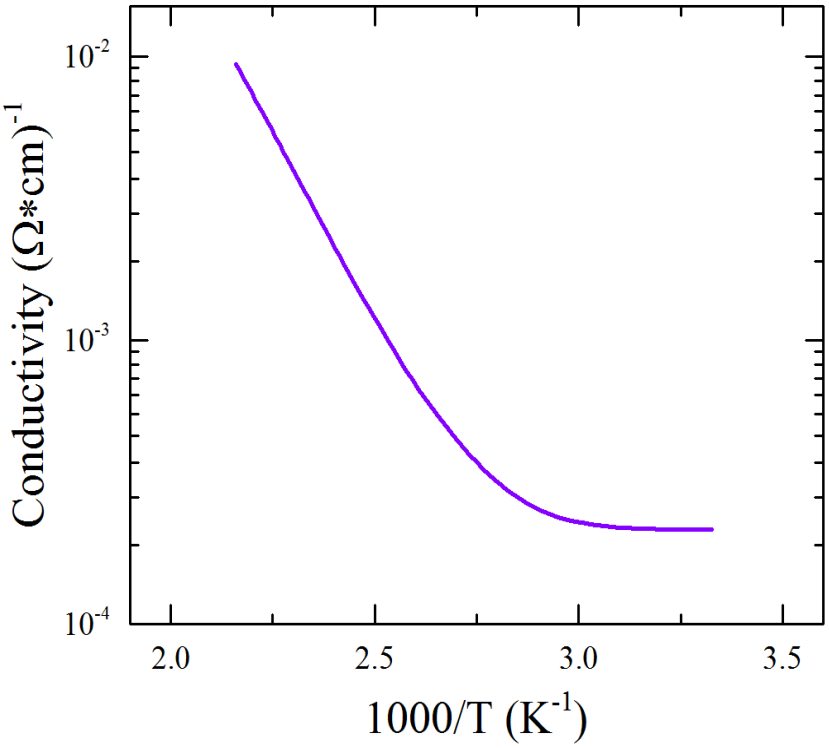

Figure 3. Arrhenius plot of crystalline silicon. Conductivity is plotted on a log scale. A linear relationship can be seen with a slope of $-E_a$, indicating thermally activated conduction. Figure courtesy Prof. Kakalios.

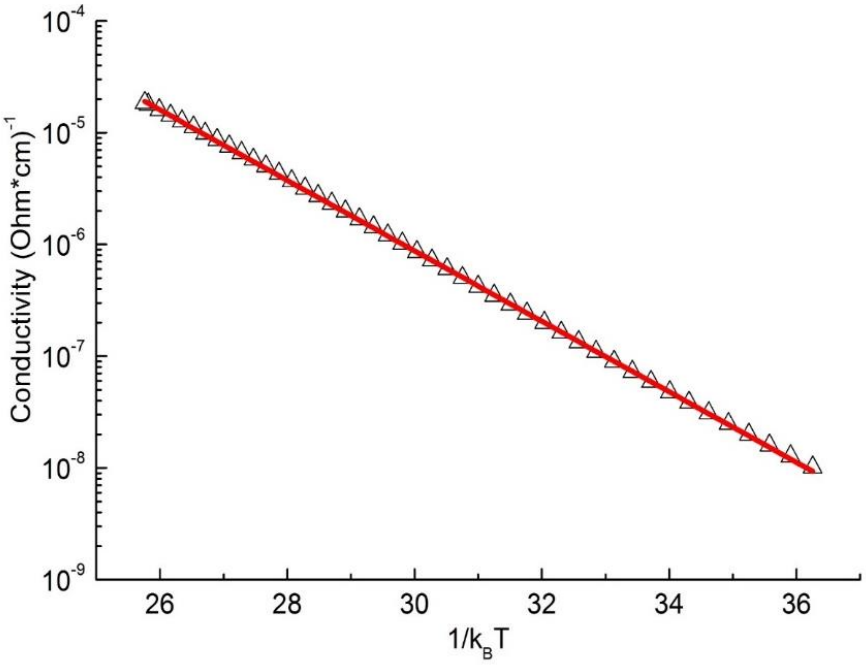

Figure 4. Arrhenius plot of amorphous silicon. Conductivity is plotted on a log scale. Again, thermally activated conduction is observed with slope $-E_a$. Figure courtesy Prof. Kakalios.

Conduction in nanocrystals occurs by percolation, where at least one path of nanocrystals in contact exists between two leads, allowing for charge transport through connected chains of nanocrystals [3]. The limiting factor in this case are the grain boundaries—conduction occurs within the nanocrystal relatively easily but charge carries must pay a price in energy in order to cross from one nanocrystal to the next. In contrast, crystalline silicon has a periodic lattice and long range order, allowing for conduction along any path.

However, close examination of an Arrhenius plot for free-standing thin films of nanocrystalline silicon, as seen below in Fig. 5, reveal deviations from linearity. When plotting conductivity data and the fit to Equation 1, the data can be seen to oscillate about the fit, indicating that conduction may be occurring by mechanisms other than simple thermal activation. In this case, the Zabrodskii analysis can be used to quantify this deviation from linearity. We can write the temperature dependence of the conductivity as

$$\sigma = \sigma_0 e^{-\left(\frac{T_0}{T}\right)^{\kappa}} \tag{2}$$

where simple thermally activated conductivity has $\kappa = 1$. Taking the logarithm of both sides, we have $\ln\sigma = \ln\sigma_0 - \left(\frac{T_0}{T}\right)^{\kappa}$, which can be expanded into $\ln\sigma = -T_0^{\kappa} + T^{-\kappa} + \ln\sigma_0$. We define the Reduced Activation Energy W as $\frac{d\ln\sigma}{d\ln T} = \frac{d\ln\sigma}{\frac{dT}{T}} = T\frac{d\ln\sigma}{dT}$, meaning that $T\frac{d\ln\sigma}{dT} = T \times (-\kappa T^{-\kappa-1})$. In this case $W = AT^{-\kappa}$ and κ tell us about the conduction mechanism. By plotting $\ln(T/T_0)$ vs $\ln W$, the slope of the line gives κ. [4] The error in κ is determined by manually fitting a line that is slightly above and a line that is slightly below all of the points, and finding their slopes. The difference between these slopes and the best fit slope is the uncertainty in the determination of the $\kappa \pm$ value. While fitting, low

temperature data (below 340K) is ignored due to the large amount of noise at the low limit of the femto-ammeter. High temperature data (between 480K and 500K) is also ignored due to the thermal lag of the system causing the actual temperature to be higher than the temperature set by the heaters.

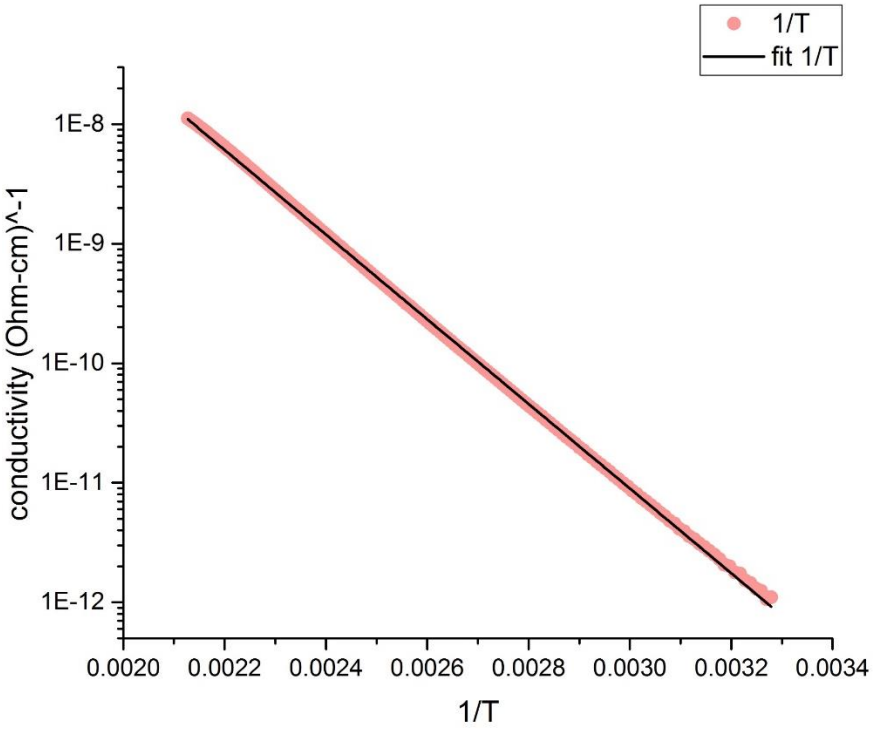

Figure 5. Arrhenius plot for nanocrystal silicon (12nm diameter). Conductivity is plotted on a log scale. Data (pink) can be seen to deviate slightly from the fit for thermally activated conduction (black line).

Previous work by the Kortshagen group studied dangling bonds in nanocrystal films. A dangling bond is a defect in which a normal Si—Si bond is broken, resulting in two bonds that are neither hydrogenated, nor connected to any other silicon atom. This inhibits conductivity through the bulk silicon, acting as traps for electrons and holes moving through the silicon. The Kortshagen group found that air exposure increased the density of defects. These defects decreased the efficiency of electronic doping and degraded light emission from nc-Si films [1].

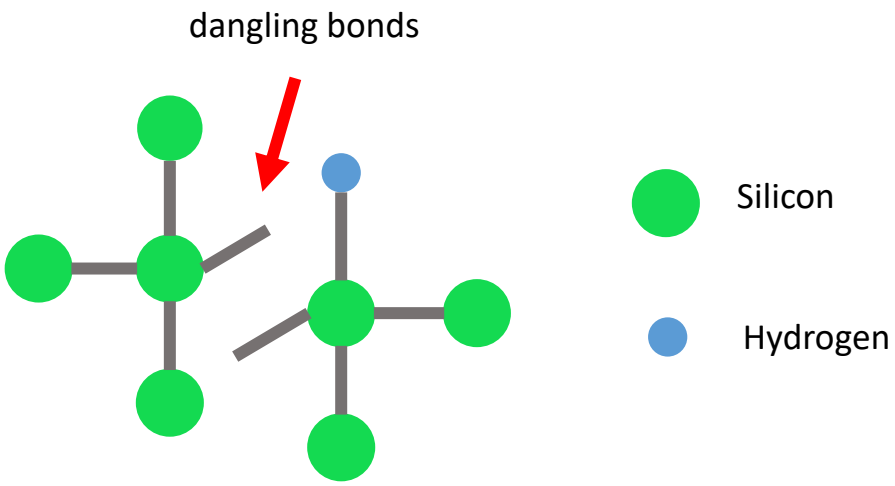

Figure 6. Example of dangling bonds. Green circles indicate silicon, blue circles indicate hydrogen.

As seen in Fig. 7 below, Kortshagen's group did not observe changes in the defect density in nanocrystals until 20 to 30 hours of oxidation. Similarly, by measuring the infra-red absorbance of oxidized silicon (Si – O – Si), increases in oxidation of the nanocrystals were not observed until about 30 hours. Nanocrystals with higher crystallinity were less sensitive to oxidation, presumably due to lower amounts of amorphous silicon, which is more susceptible to dangling bonds [1].

Interest in these studies prompted Brendon Jones, also working with Prof. Kakalios, to study the effects of atmosphere exposure on conductivity on 12 nm diameter crystals, looking at the effects of introducing defects on a timescale similar to that observed by the Kortshagen group. This work was continued by Jake Novotny on shorter timescales but with a sample consisting of free-standing nanocrystals with the same diameter. Interest in studying the effect of dangling bonds on nanocrystal size is the motivation of this work. Comparisons between previous data of 12 nm crystals and new data of 5.5 nm crystals will be made, in both the decay of conductivity and changes in the conduction mechanism.

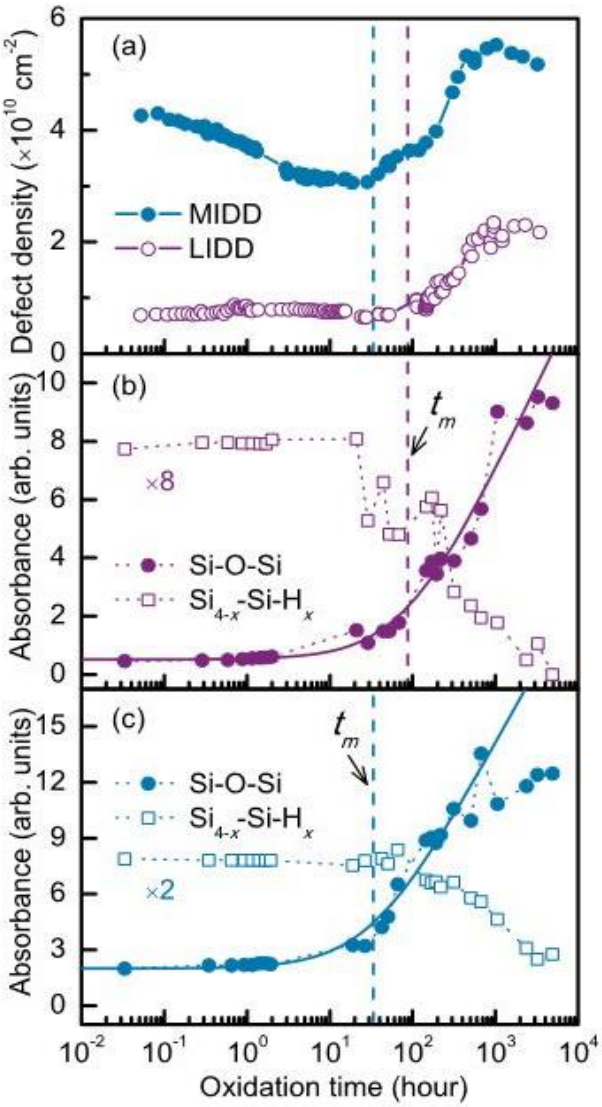

Figure 7. Effect of oxidation on silicon nanocrystals. Top graph shows changes in defect density for high and low crystallinity silicon. Middle and bottom graph show changes in the absorbance of Si-O-Si with respect to oxidation time. FTIR and ESR are used for measurement. Image from Pereira, et. al. [1]

Procedure

The nanocrystals are synthesized using Plasma Enhanced Chemical Vapor Deposition (PECVD). In this process, a reactant, silane (SiH_4), and a carrier gas, argon, are introduced into a plasma deposition chamber and allowed to mix. The reactant is ionized by the argon plasma, and broken up into silicon and hydrogen atoms using radio frequency power. The silicon atoms then form into nanoparticles, which are bombarded with argon ions. This causes the particles to melt and re-crystallize, forming nanocrystals. The size of the nanocrystals is dependent on the flow rate of gas through the chamber. Faster flow rates allow for fewer collisions, and the particles exiting the chamber are smaller. Exiting particles are carried out through a nozzle by the argon gas. Deposition occurs onto two metal electrodes attached to a glass slide placed below the chamber. A piece of tape is used to cover the ends of the electrodes to prevent the nanocrystals from covering the entire electrode. After the nanocrystals are deposited, the tape is removed to allow for contact to measurement leads [5, 6]. Fig. 8 is an example of a PECVD chamber [4].

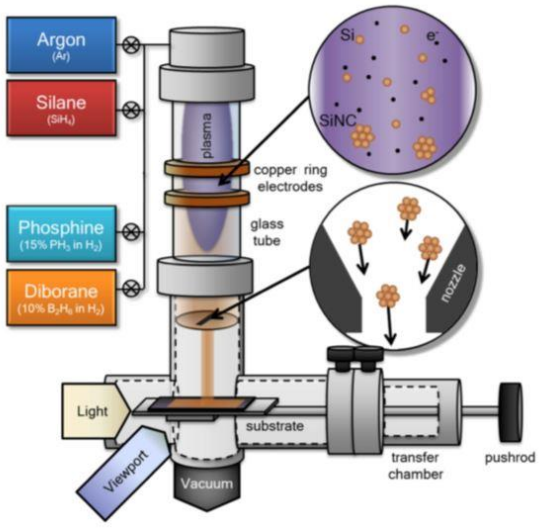

Figure 8. Example of a plasma enhanced chemical vapor deposition system. Image courtesy Brendon Jones [4]

The resulting nanocrystals have a fully crystalline center. Remaining dangling bonds on the surface attach to free hydrogen, and form a hydrogenated amorphous shell. The crystallinity of the nanocrystals is dependent on the flow rate of gases and specific mixture of reactants. Crystallinity is confirmed using Raman Spectroscopy, probing the difference between silicon-hydrogen bonds and silicon-silicon bonds. Raman spectra of crystalline and amorphous silicon can be compared to distinguish crystallinity of nanocrystals, where crystalline silicon, having mostly Si-Si bonds, has a narrow peak and amorphous silicon, with both Si-H and Si-Si bonds, has a broad peak (Fig. 9). Higher crystallinity silicon produces Raman spectra closer to crystalline silicon.

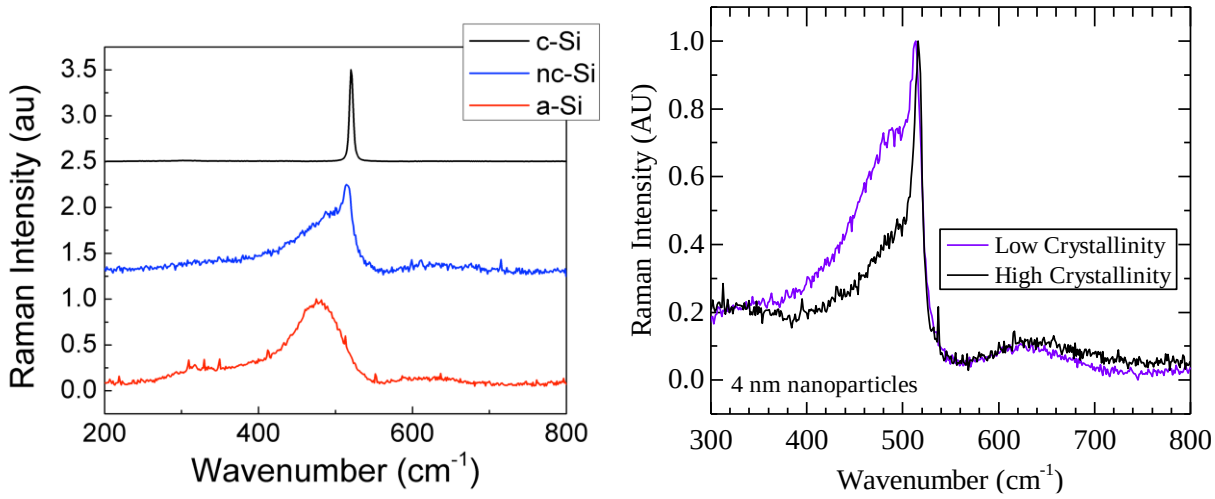

Figure 9. Raman spectra of crystalline, nanocrystal, and amorphous silicon (left). Raman spectra of high vs low crystallinity nanocrystals (right). Figures from Wienkes [7].

Nanocrystal size is confirmed using X-Ray Diffraction. Larger crystals have more crystal planes, providing more planes with equal path difference, causing more deconstructive interference and narrower peaks, as seen in Fig. 10.

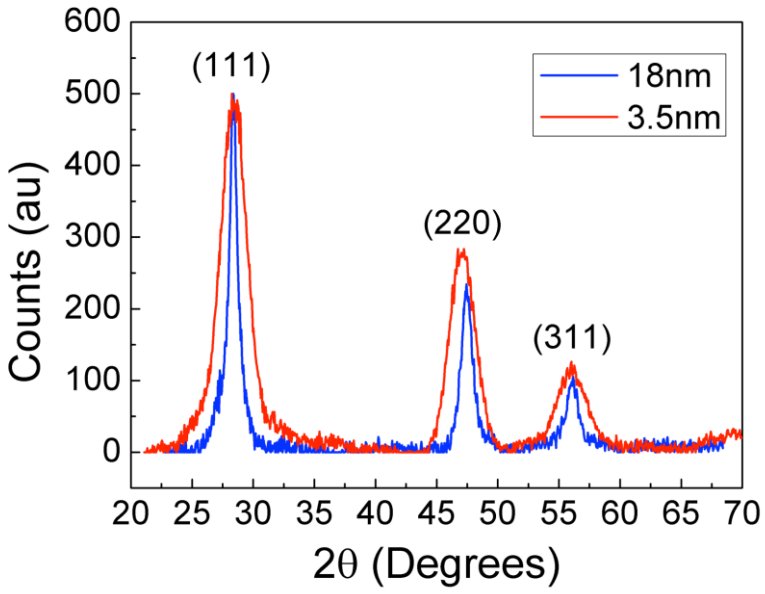

Figure 10. X-Ray Diffraction spectra of nanocrystal silicon, with Bragg angle as the x-axis. Larger crystals have narrower peaks. Figure from Wienkes [7].

After the sample is deposited onto the substrate in the PECVD chamber, it is moved into the measurement apparatus as quickly as possible and placed inside a vacuum chamber pumped down to the milliTorr range (Fig. 11). It is secured to a copper block and the measurement leads using silver paint. The block contains a heating element, allowing the sample to undergo temperature ramping. There is a window at the top of the measurement chamber, normally covered when the sample is not undergoing a light-soak. Example of a sample with tape still covering the electrodes is seen in Fig. 12.

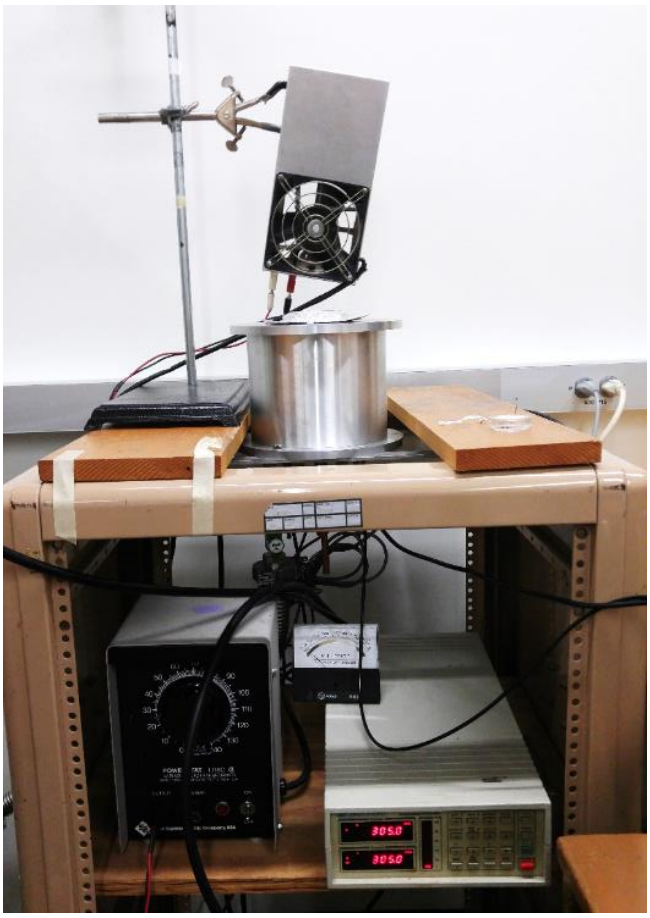

Figure 11. COND2 Measurement apparatus. Sample is placed inside silver chamber.

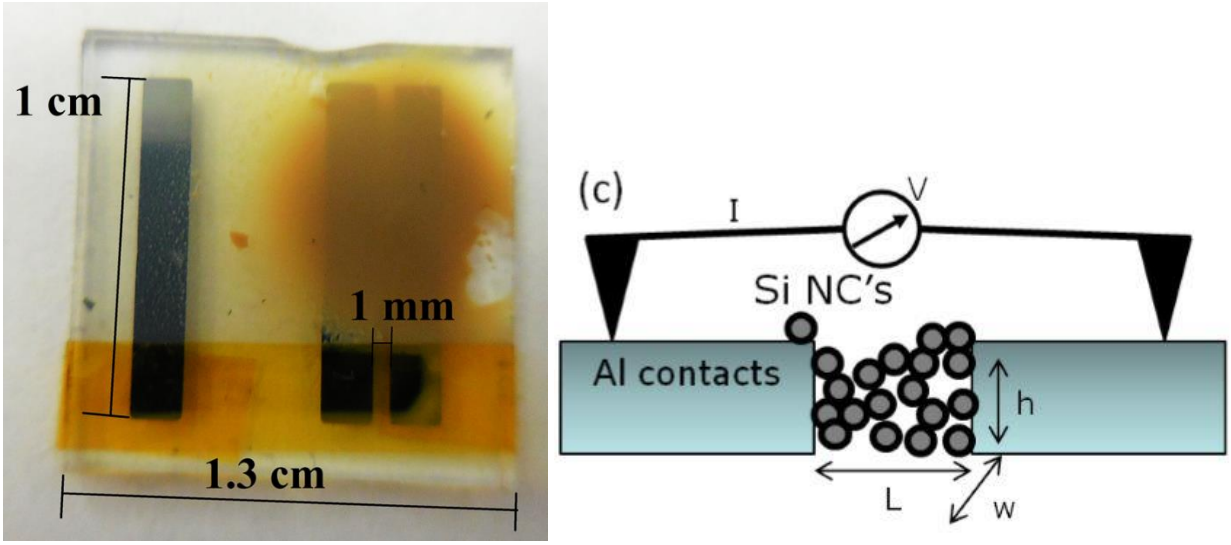

Figure 12. Nanocrystals deposited on glass slide with electrodes (left). Cross-sectional view of deposited nanocrystals on glass surface (right). Images courtesy Prof. Kakalios.

The conductivity is measured with an applied voltage of 50 Volts while the temperature is ramped from 305K (room temp) up to 500K at a rate of one Kelvin per minute. After ramping, the sample is annealed at 500K for two hours, and cooled slowly down to room temperature. Previous studies stopped at a maximum temperature of 470K, and the maximum temperature of the heater is around 518K. Thermal lag is present in the system, causing the highest temperature data points during the ramp down to show temperatures higher than actually present in the system. These points are excluded from the data analysis.

The sample was exposed to atmosphere between each measurement. Since the film is freestanding, care was taken to prevent the film from being disturbed by air rushing into the chamber. The valve is located beneath the heating block, so no direct air currents affect the film upon venting the chamber. The valve to the vacuum pump was first closed, while the atmosphere valve was opened slowly, over the course of three minutes, while watching the pressure gauge. When closing the sample to atmosphere, the valve is closed immediately while the vacuum valve was opened slowly over the course of ten minutes to prevent shocking of the vacuum pump and to prevent sudden air currents from disturbing the sample.

Results

Decay in Conductivity

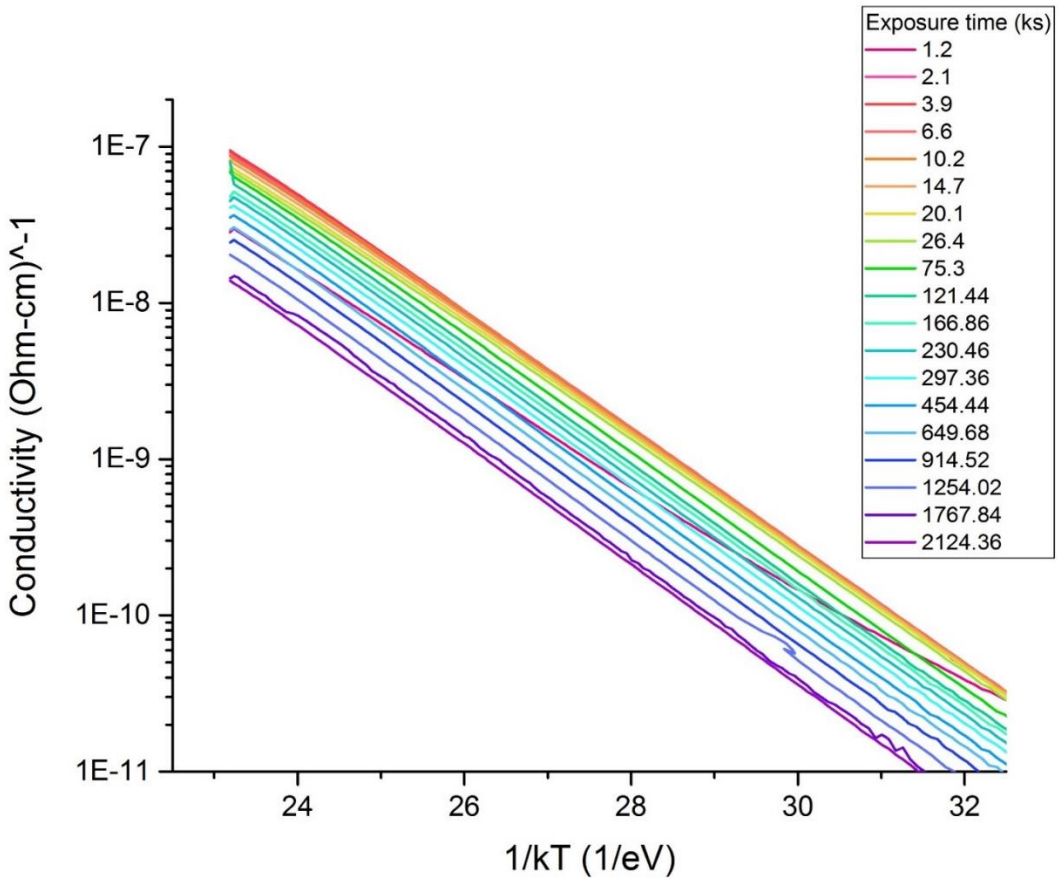

Figure 13. Arrhenius plot of all decreasing temperature measurements. Increasing exposure time corresponds to decreasing conductivity. The first measurement does not follow this pattern, but a subsequent measurement with the same exposure time does.

As the film is exposed to atmosphere, the dark conductivity measured when the measurement chamber is re-evacuated and following a high temperature anneal, decreases at all temperatures. A comparative Arrhenius plot of all samples is seen in Fig. 13. To model the decay, conductivity at 340K was measured. A stretched exponential of the form $\sigma = \sigma_0 e^{-t/\tau}$ is seen with $\beta = 0.4$ as the best-fit parameter, $\tau = 255\ ks$, and $R^2 = 0.983$, as seen in Fig. 14.

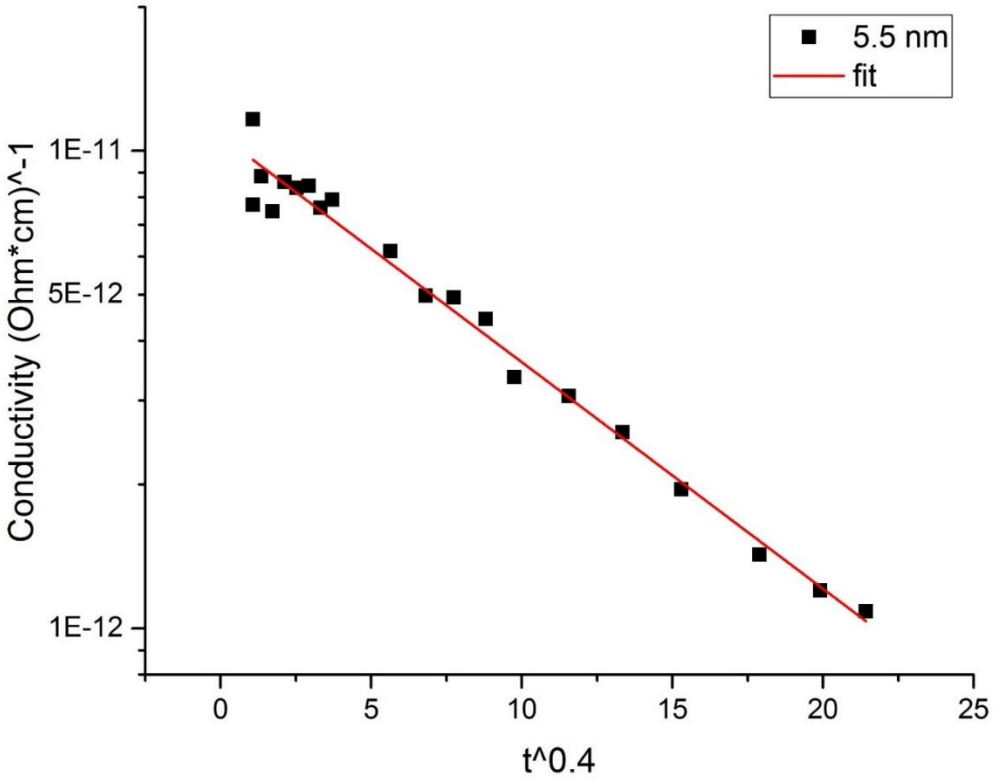

Figure 14. Stretched exponential decay of 5.5 nm nanocrystal conductivity. Here the x-axis is time in ks to the power of 0.4 and the y-axis is conductivity in log scale. Fit is seen in red.

Similar β and τ are seen at 380K, indicating that conductivity decrease is consistent at all temperatures. This is a marked difference from previous data for 12 nm nanocrystals, where exponential decay and power law decay of conductivity are seen. In Brendon's work on 12 nm nanocrystals, exponential decay of the form $\sigma = \sigma_0 e^{-t/\tau}$ is seen, with $\tau = 510\ ks$ and $R^2 = 0.984$ as shown in Fig. 15. Here, the conductivity levels off to $\sigma(t = \infty)$, where $\sigma(\infty)$ was the conductivity of an identical sample left out on a lab bench, open to atmosphere for one year, considered to be the baseline conductivity of the sample.

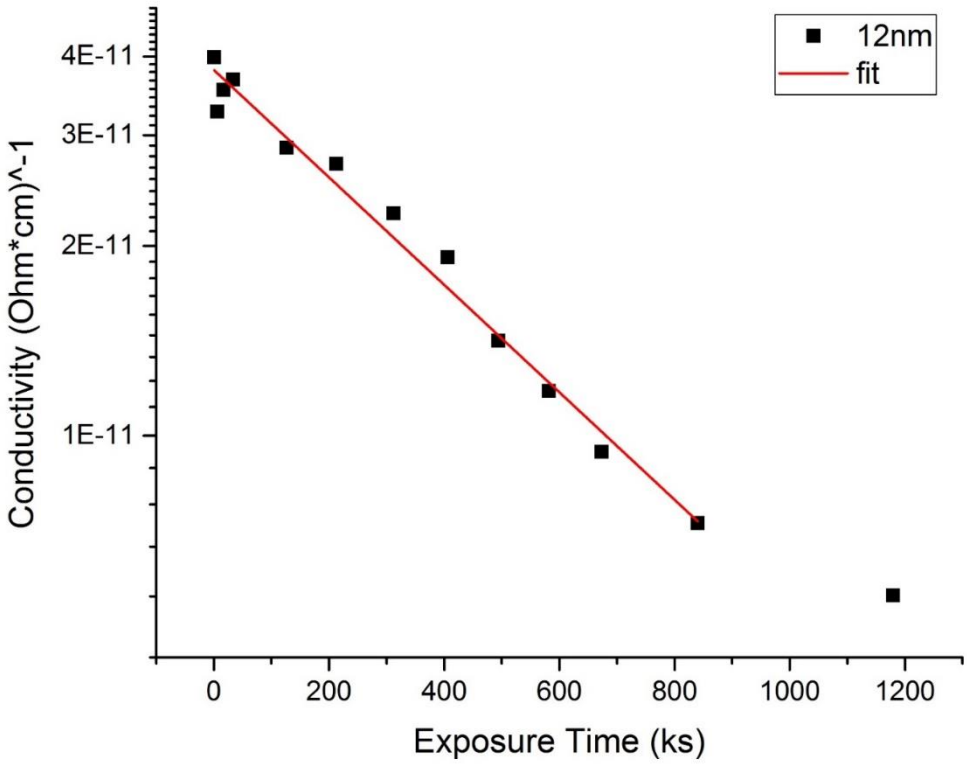

Figure 15. Exponential decay of conductivity for 12 nm nanocrystals. Conductivity plotted on log scale. Fit is seen in red. Data taken by Brendon Jones.

Power law decay of the form $\sigma = \sigma_0 \left(\frac{t}{\tau}\right)^{-m}$ is seen for the shorter timescale 12 nm sample, with $m = 0.32$, $\tau = 0.6\ ks$, and $R^2 = 0.982$ in Fig. 16. However, lack of longer timescale measurements on this sample means that we are not confident that the fit would remain a power law at long exposure times. Nevertheless, comparing data points for similar exposure times showed the three decay models to be distinct.

Another possible decay mechanism considered was the expression: $\sigma = \frac{\sigma_0}{1+(t/\tau)^{\gamma}}$ where $\gamma = 2$ for dispersive biomolecular recombination. The best fit had $\gamma = 0.75$ with $R^2 = 0.994$, in Fig. 17.

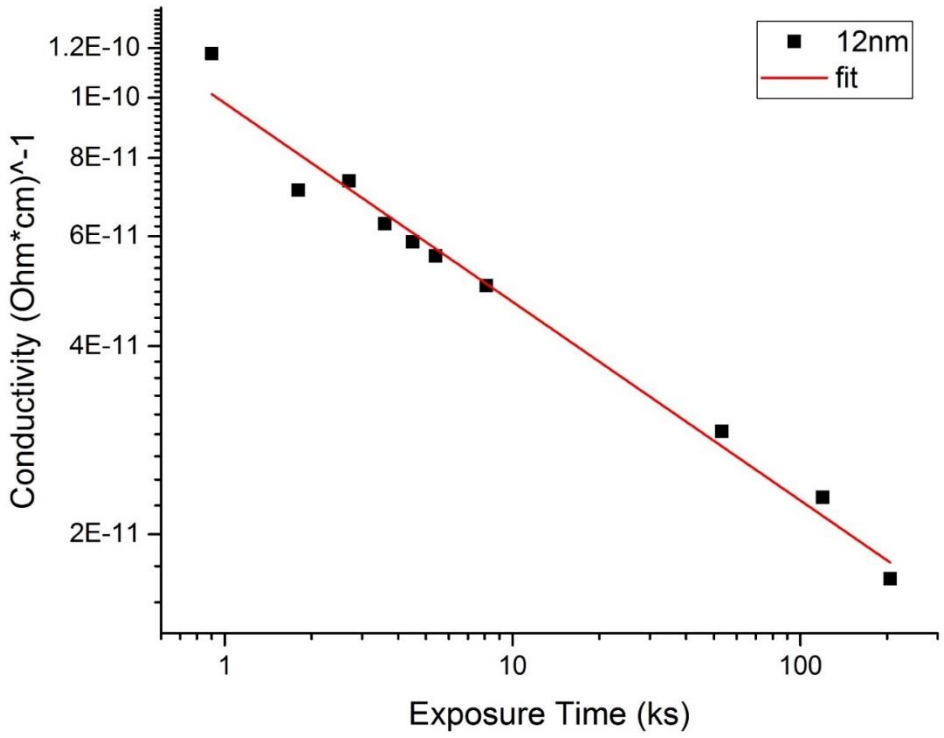

Figure 16. Power law decay of conductivity in 12 nm crystals. Conductivity shown in log scale. Fit is seen in red. Data taken by Jake Novotny.

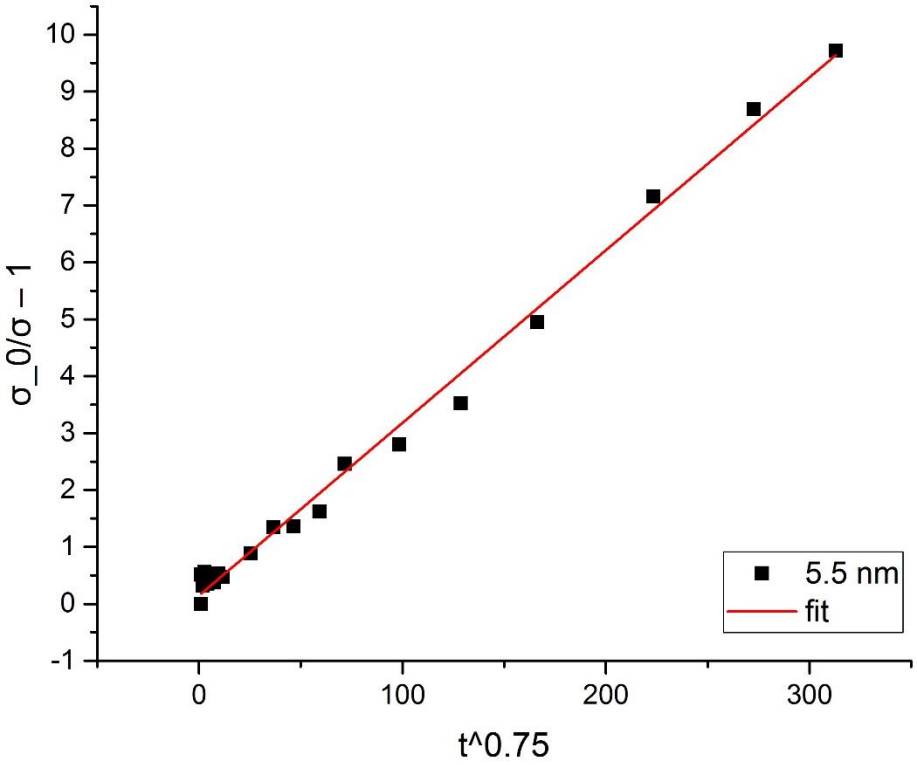

Figure 17. Attempt to fit dispersive molecular recombination on the 5.5 nm nanocrystals did not produce the correct γ. Fit seen in red.

Comparing the exponential and stretched exponential fits, we have only two nanocrystal sizes. Further measurements with crystal sizes between 5.5 nm and 12 nm could provide more information on how the β parameter in a stretched exponential is related to size. A regular exponential decay has $\beta = 1$, as seen in Fig. 18 in comparison to a stretched exponential with $\beta = 0.4$. No explanation is currently available for why a different β is seen for the smaller nanocrystals.

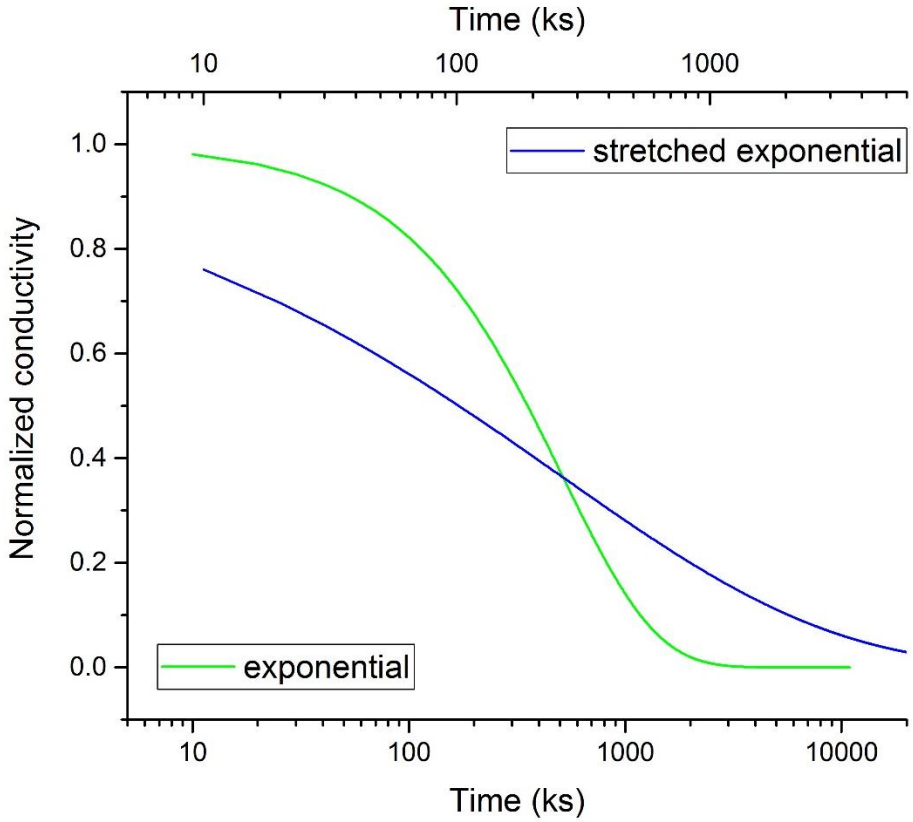

Figure 18. Comparison of exponential and stretched exponential ($\beta = 0.4$) *decay. Functions cross at time* $t = \tau$*, where* $\sigma(\tau) = e^{-1}$.

Plotting all three samples on the same figure shows the distinct decay functions (Fig. 19). The conductivity of the free-standing nc films is determined by percolation processes, and is lower for smaller nanocrystals due to the larger surface area to volume ratio causing for less of the conductivity to occur within the completely crystalline region of a nanocrystal.

No explanation can be found for why one 12 nm nanocrystal sample had a much larger σ_0 than the other, though these films were made at different times, despite having the same PECVD deposition conditions. More studies concerning the reproducibility of these results is warranted.

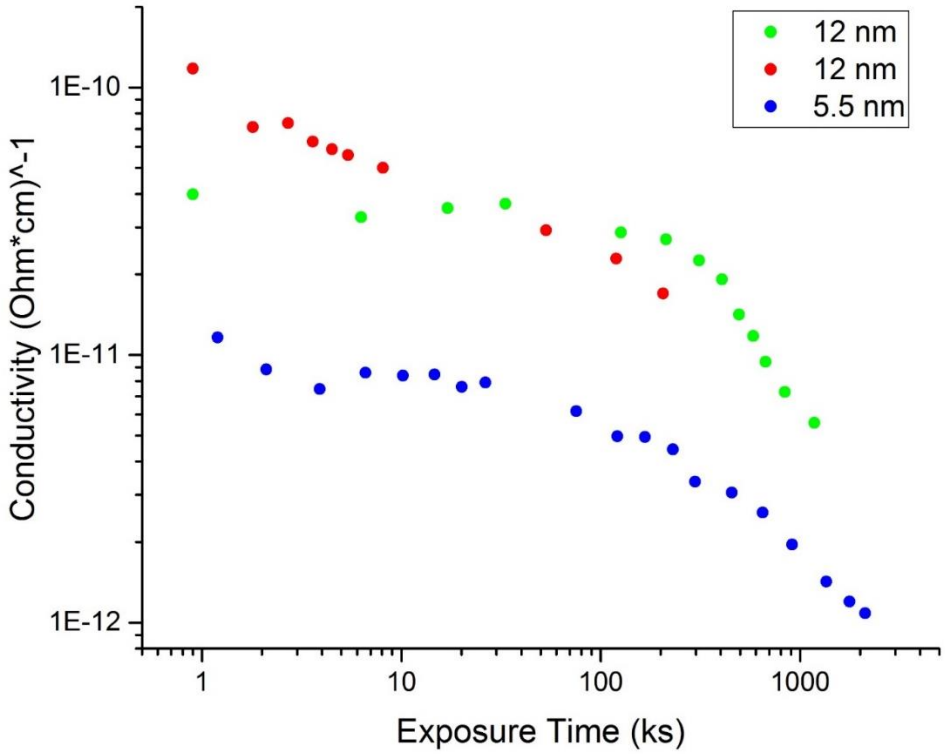

Figure 19. Conductivity data for all three samples at 340K. Both exposure time and conductivity are plotted on a log scale.

Changes in conduction mechanism

The Zabrodskii Reduced Activation Energy analysis allows us to investigate whether the conduction mechanism in this free-standing nc film changes with increasing air exposure. An example of a Zabrodskii plot is shown in Fig. 20. Here, the temperature and reduced activation energy W are both plotted on a log-log scale. At low temperature, the conductivity is so low that the data is dominated by noise (current reaches the lower

measurement limit of the femto-ammeter), and at high temperature, thermal lag is observed for decreasing temperature measurements (as shown here). The slope is clearly greater than one, indicating possible non-Arrhenius behavior or prefactor temperature dependence. The peak at $\sim 460K$ is due to the femto-ammeter switching amplifiers, and is present as an artifact at all data at the same current.

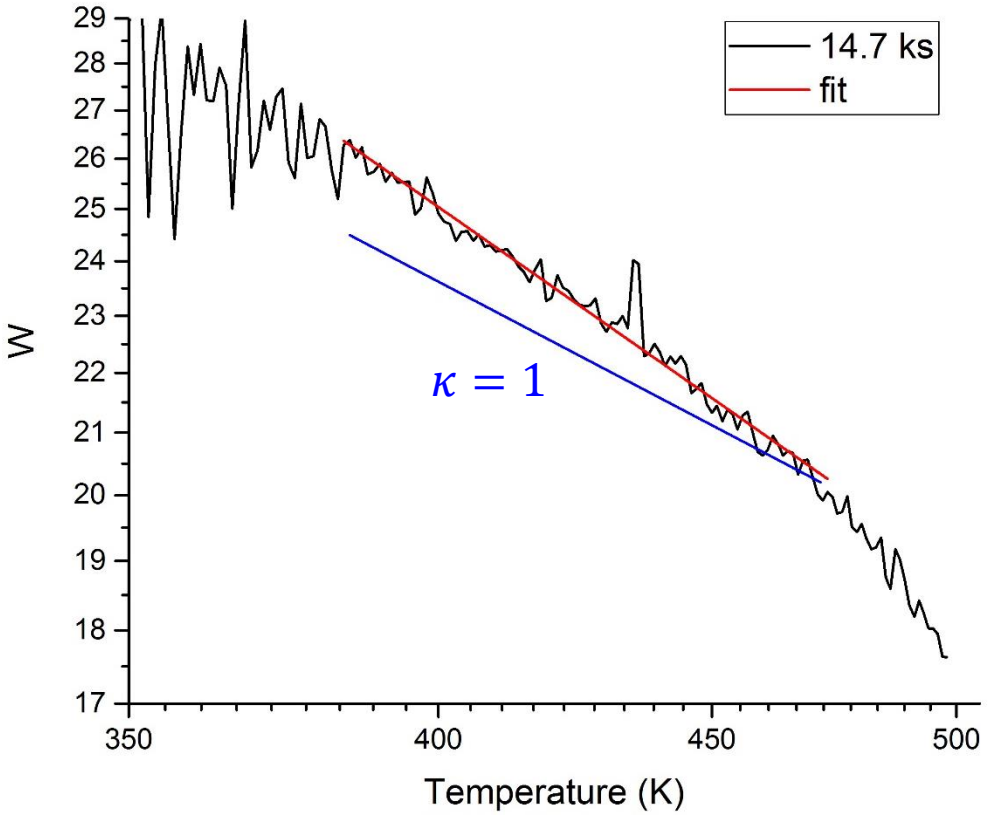

Figure 20. Zabrodskii analysis plot. Fit shown in red, $\kappa = 1$ *shown in blue, data in black.*

While a value of $\kappa > 1$ is unphysical, it is possible that the Zabrodskii plot is consistent with a simple thermally activated conductivity, with a pre-exponential factor that is strongly temperature dependent. That is, the conductivity is given by $\sigma = \sigma_0 e^{-(E_a/kT)^{\kappa}}$ where $\sigma_0 = N_C(E_C)kT^m e\mu$, or $\sigma \sim \sigma^* T^m$. Simulations carried out by Paul Friedrichsen showed that for $\kappa = 0.75$ in order for a Zabrodskii plot to yield $\kappa \sim 5/4$, the

pre-factor temperature dependence would be $m \sim -3$. This implies that the resistivity would be of the form $\rho = cT^3 e^{E_a/kT}$ with c being a constant.

Measurements made as the temperature is increasing yields drastically different results. In some cases two distinct linear regions, as seen in Fig. 21, were observed while other times a slope closer to $\kappa = 0$, was seen (Fig. 22). In Fig. 21, $\kappa = 0.75 \pm 0.03$ and $\kappa = 0.32 \pm 0.04$ are observed. The inflection point at 450K is far above the boiling point of water, excluding this transition as being due to the removal of adsorbed water. Thermal lag is not observed while increasing temperature. In Fig. 22, $\kappa = 0.17 \pm 0.2$ is seen. Noisy data is excluded from the fit. Both measurements were taken as the temperature ramped up following a high-temperature anneal.

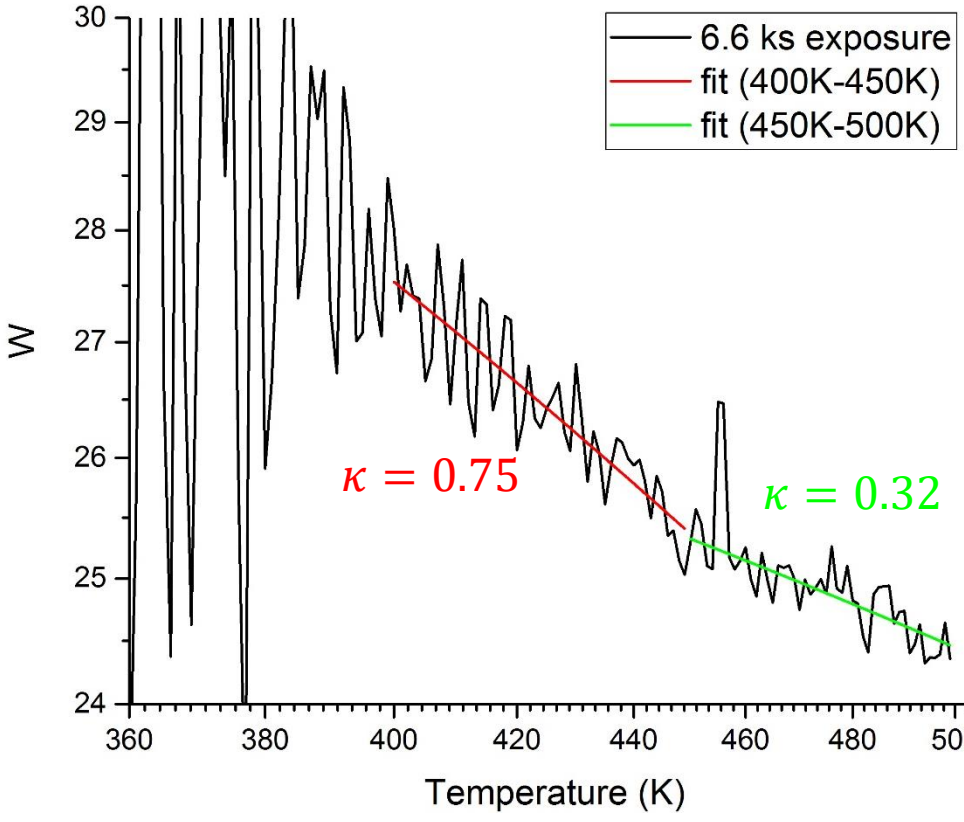

Figure 21. Increasing temperature data, with different κ. Temperature and reduced activation energy plotted on log scale.

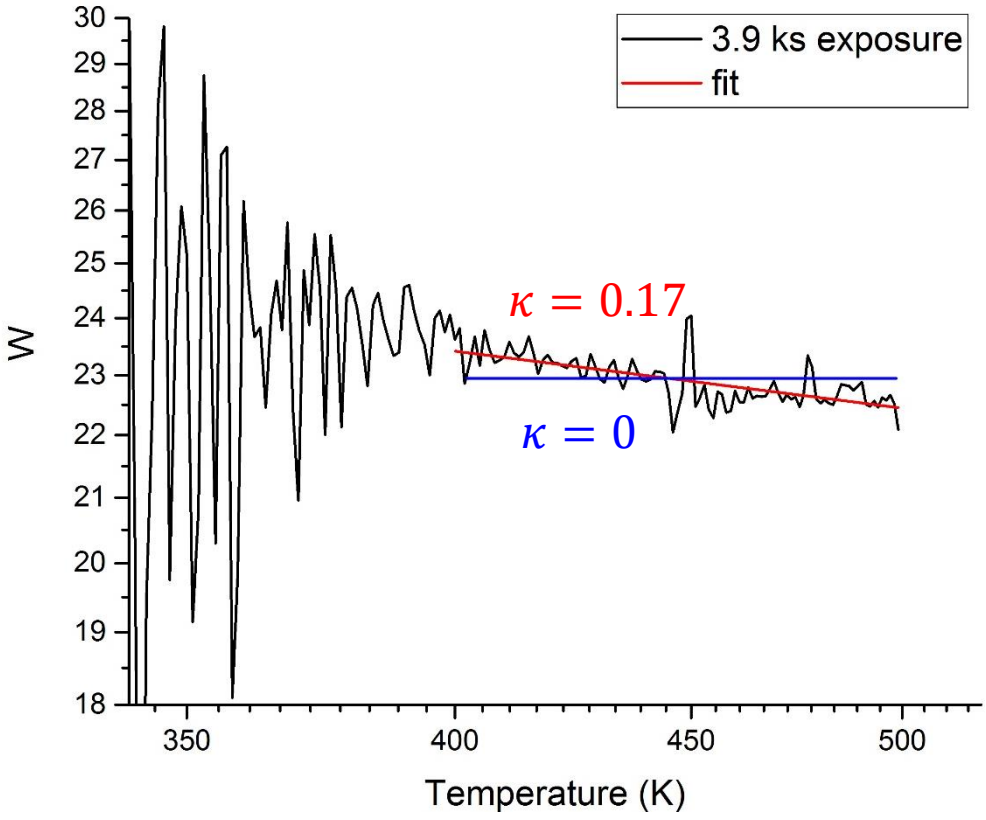

Figure 22. Increasing temperature measurement, with both temperature and reduced activation energy W plotted on log scales. Fit shown in red, and $\kappa = 0$ *shown in blue.*

To find the error on these fits, lines are drawn in by hand for fits just missing the data above and fits just missing the data below. The variation in slope is taken as the uncertainty in κ.

Comparing fits made with finding κ from the Zabrodskii analysis showed slight improvements in overall errors, as seen in Fig. 23. The pink line assumes $\kappa = 1$, while the green line assumes $\kappa = 1.24$. The fit (black) looks better on the data after the Zabrodskii analysis.

However, unlike analysis conducted previously with nanocrystalline Germanium doped amorphous silicon, errors with adjusted fits still showed a pattern, indicating that κ is still not a great descriptor of conduction occurs in the nanocrystals, as seen in Fig. 24 [8].

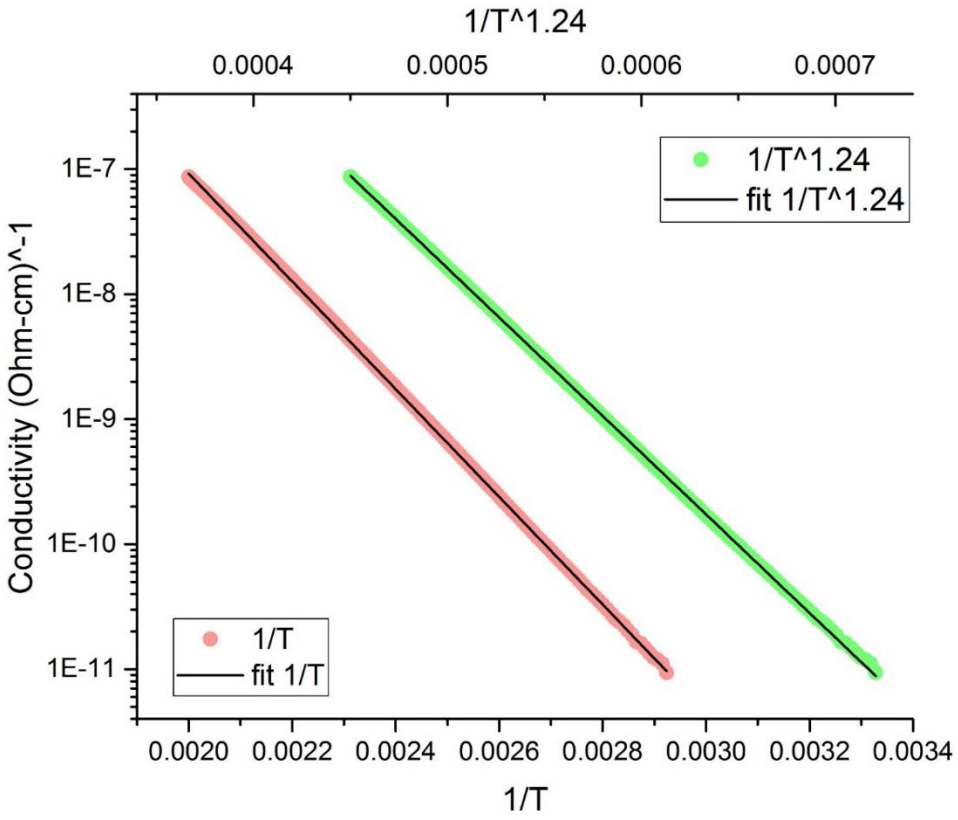

Figure 23. Comparison before (pink) and after (green) Zabrodskii analysis. Slight improvements in fit are seen.

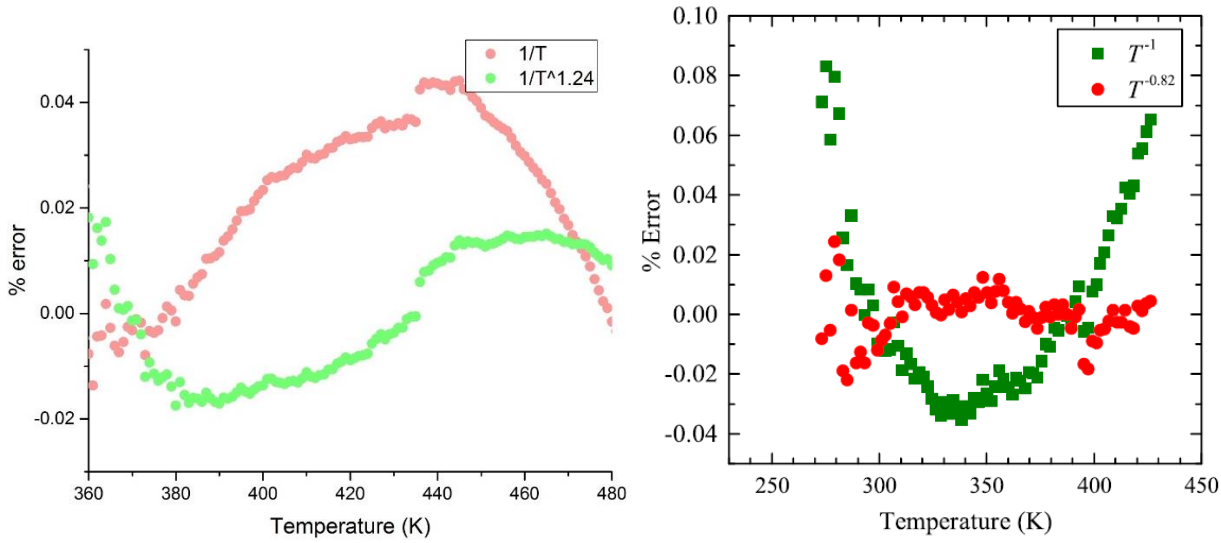

Figure 24. Errors after Zabrodskii analysis in silicon nanocrystals (left) and germanium nanocrystal doped amorphous silicon (right). Figure from Bodurtha, et. al. [8]

As the sample was exposed to air, changes in κ were observed (Fig. 25). However, all three samples showed differences in how the conduction mechanism changed. For 5.5 nm nanocrystals, κ remained close to or above 1, starting around 1.2 to 1.3 and finally settling down to around $\kappa = 1$. The two 12 nm samples previously studied showed κ values that start close to 0 for low air exposure times and increased to 1 as the cumulative time the film was exposed to air increased, but at vastly different rates. The data of Jones and Novotny was re-analyzed using the methods described here (excluding the same amount of noise, error determination) to allow for comparison.

Kappa values near zero could indicate multiple phonon hopping conduction, seen previously in amorphous silicon. Observations of such values suggests that a significant amorphous shell surrounding each particle limits conduction between nanocrystals.

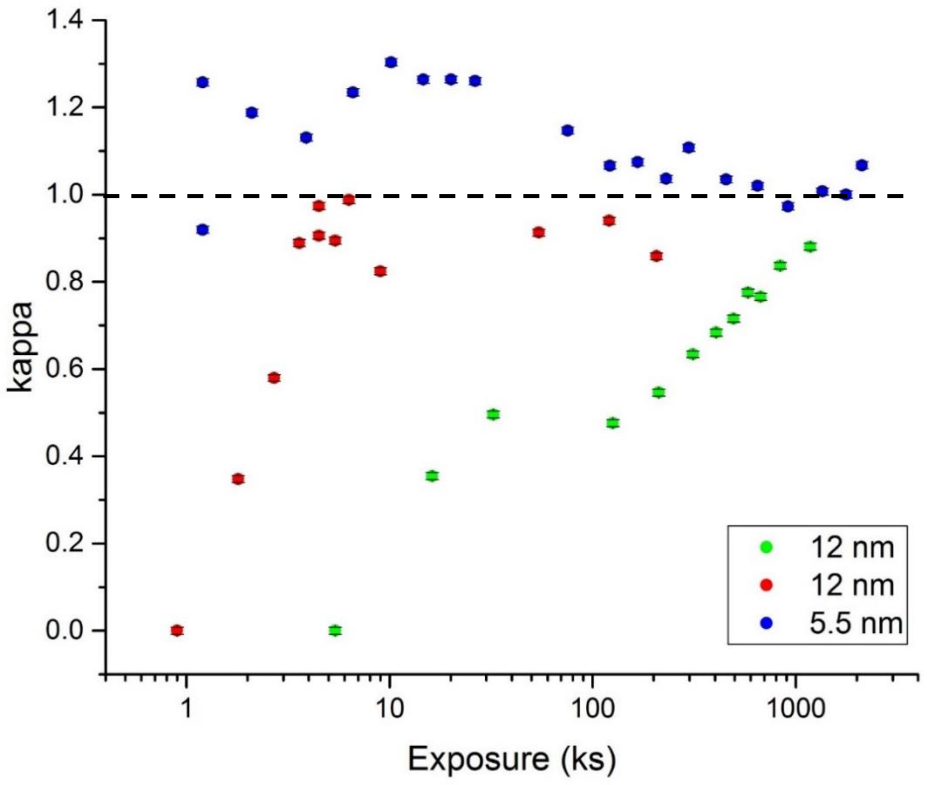

Figure 25. Comparison of κ for all nanocrystal sizes measured. Dashed line shown at $\kappa = 1$ for expected Arrhenius behavior.

Reliability of measurements

Experiments were conducted to determine whether or not temperature ramping measurements are reliable, since only one such measurement is made before the sample is exposed to atmosphere and changed. An example of the program used to test repeatability is shown in Fig. 26. All temperature ramping between 305K and 500K takes place at the rate of 1K/minute, so ramping measurements take 3.25 hours. All anneals (at 500K) and all rests at room temperature (305K) are two hours long, with the exception of the final anneal which is four hours. Each temperature ramping step (up or down) is labeled between 1 and 16. This program was run twice in its entirety.

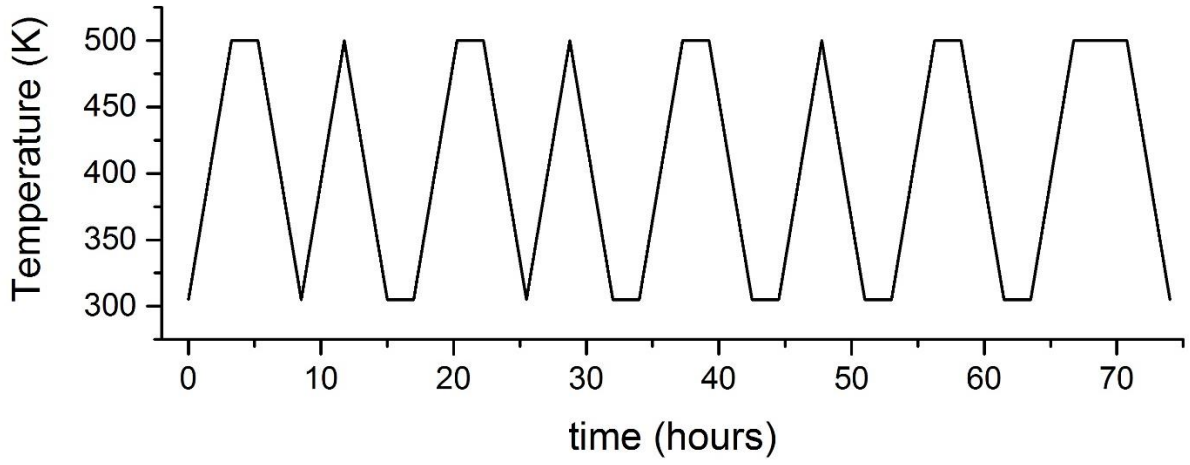

Figure 26. Repeatability test temperature ramping program. A total of 16 steps (not including anneal or rest) are measured.

Steps 1-4 and 5-8 have exactly the same procedure and occur under the same conditions without any change in between. This measurement program was the original method for all oxidation studies. By observing differences between these two, we can determine how reproducible previous measurements were.

As shown in Fig. 27, slight differences are observed between the first set and the second set of temperature ramps. The largest differences are seen between steps two and six, the decreasing temperature measurements directly after annealing. These differences are reduced in the subsequent steps, between 3 and 7, and 4 and 8. These small differences in conductivity were consistent between both runs of the program.

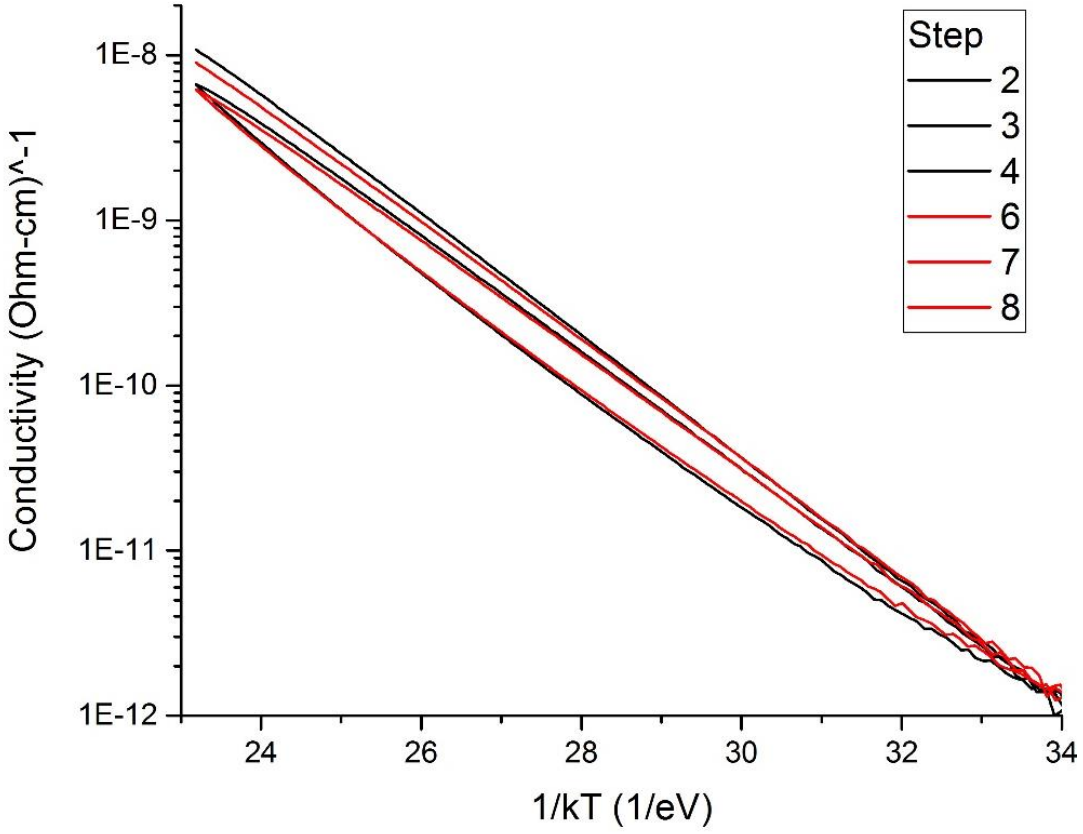

Figure 27. Comparison of set 1 (black) and set 2 (red) Arrhenius plot. Slight differences in conductivity are observed. This data is typical of such measurements.

By comparing between the two identical runs of the program, as seen in Fig. 28, differences are observed. All increasing temperature measurements have κ between 0 and 0.2, with an uncertainty of 0.2. All decreasing temperature measurements have much higher κ values, between 1 and 1.3, with uncertainties of around 0.05. The observed κ are higher than previous studies (shown as step 0). In previous work by Jake Novotny, κ of decreasing

temperature measurements directly following the first anneal after atmospheric exposure are lower than subsequent measurements. Since these data were taken without exposure to atmosphere, this was expected.

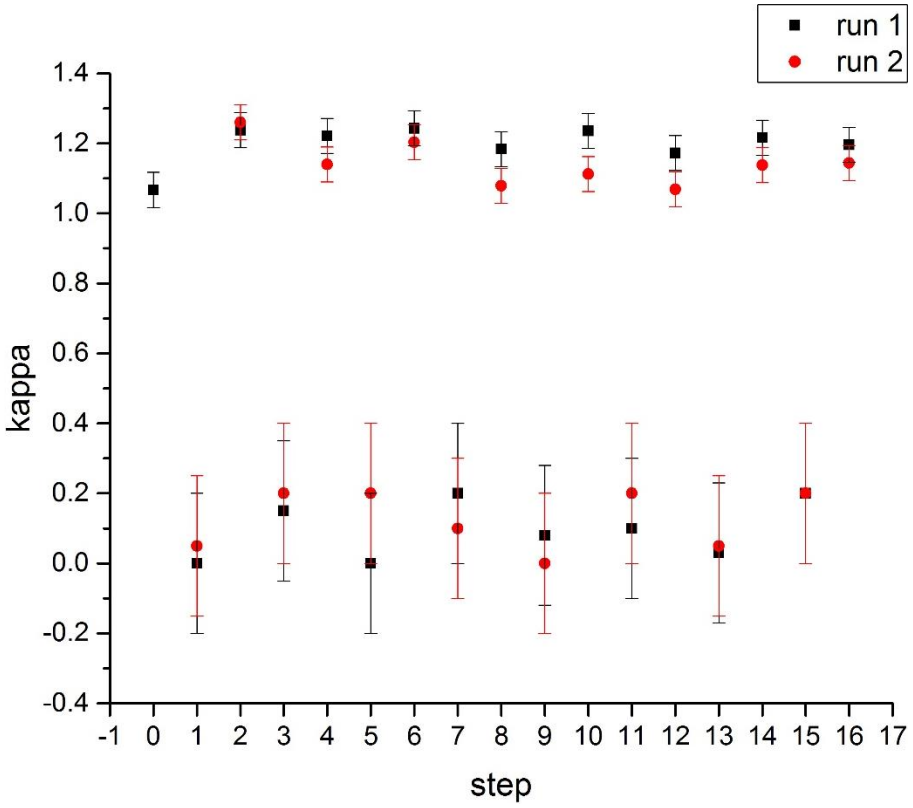

Figure 28. Comparison of κ between the two runs. Run 1 seen in black, run 2 seen in red.

It is interesting to note that for decreasing temperature measurements, Fig. 29, all of the first run data (in black) seem to have higher κ than the second run data (in red). The two runs were separated by an attempt to take the system to higher temperature (600K), but the heater peaked at 518K. Thus the only difference between these two measurements was taking the sample to a slightly higher temperature than previously attempted (for all of the other data presented here, the highest anneal temperature is 500K).

More measurements would be needed to determine the statistical significance of these differences from run to run. Patterns can be observed for decreasing temperature measurements. It can be seen that $\kappa(2) > \kappa(4)$ in both runs, and the same holds for $\kappa(6) > \kappa(8)$ and $\kappa(10) > \kappa(12)$. This pattern shows that κ of a decreasing temperature measurement directly after a two hour anneal is larger than the κ of a decreasing temperature measurement directly after an increasing temperature measurement.

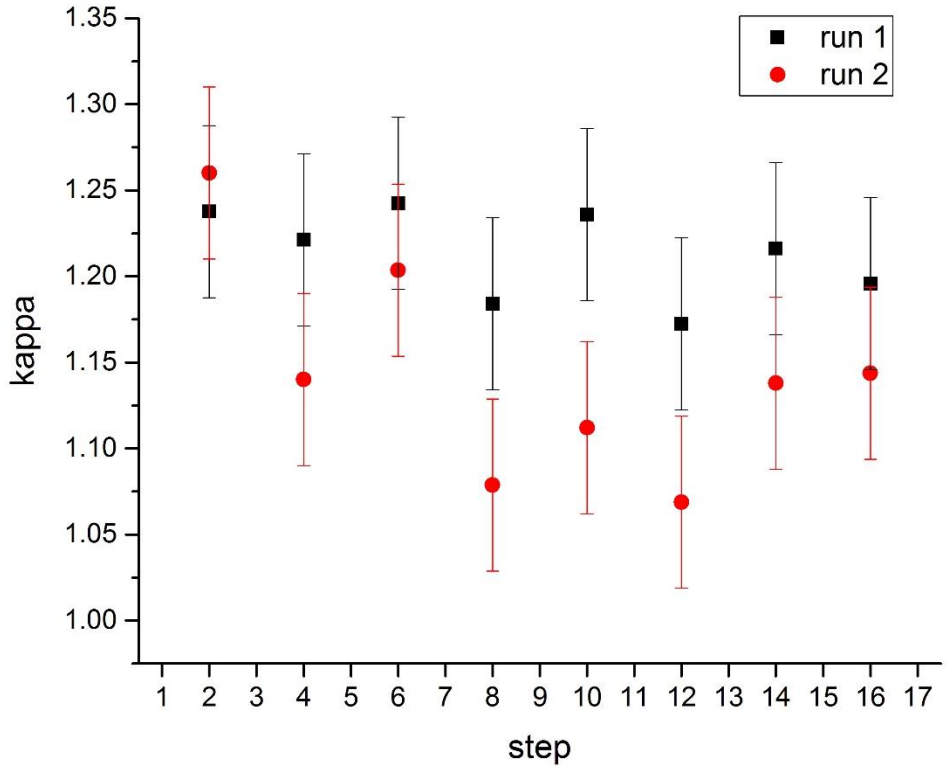

Figure 29. Decreasing temperature measurements.

Since all increasing temperature measurements produced much lower κ values compared to those obtained from decreasing temperature measurements, it may be the result of different conduction mechanisms.

Summary

The conductivity of a 5.5 nm freestanding silicon nanocrystal film was measured as a function of temperature for increasing oxidation time, for a final total oxidation time of 2124.36 ks (about 24.5 days). Unlike previous work on defect density in nanocrystal films by the Kortshagen group, changes in conductivity were observed in the nanocrystal film immediately upon exposure to atmosphere as opposed to after 30 hours of exposure. This appears to be consistent with previous work on 12 nm films where decreases in conductivity were immediately observed. However, comparisons made between 5.5 nm and 12 nm silicon nanocrystals showed marked differences in the decay of dark conductivity at 340K. The decay model of the 5.5 nm nanocrystal followed a stretched exponential form, with stretching exponent $\beta = 0.4$ and time constant $\tau = 255ks$. Previous work showed 12 nm crystals to follow exponential decay and power law decay. Measurements of an intermediate nanocrystal size could clarify how these models are related, but no explanation of these models can currently be found.

By conducting the Zabrodskii analysis, comparisons of conduction mechanism between the different nanocrystal sizes were also made. Calculations showed κ inconsistent with thermally activated conduction ($\kappa > 1$). One explanation for this could be a higher power temperature dependence of the conductivity prefactor σ_0, which would indicate thermally activated conduction but with other properties present. Furthermore, measured κ for 5.5 nm nanocrystals showed κ always greater than or around $\kappa = 1$, whereas previous measurements on 12 nm nanocrystals showed κ starting close to zero and increasing to $\kappa = 1$, albeit at different rates. It is possible that the rate of κ increase was much higher in the smaller nanocrystals, thus causing the observed initial value to be

greater than $\kappa = 1$. These measurements would also be bolstered by the addition of an intermediate size nanocrystal, both to observe the initial κ and also to observe how quickly κ rises to $\kappa = 1$ with exposure time.

Differences were observed between increasing temperature measurements and decreasing temperature measurements, with κ close to zero for increasing temperature and higher than one for decreasing temperature. This could indicate changes in conduction mechanism due to the process of anneal, potentially providing a reservoir of phonons or other changes to the electronic state of the system. The measurement of $\kappa = 0$ indicating no dependence on temperature is unexpected and no explanation is found yet.

Measurements made to gauge reliability of the system showed slight changes between identical measurement methods. More repeats of this program would result in better statistical analysis on the precision of the conductivity measurements. Changes observed in κ showed that κ was higher after a two hour anneal as opposed to no annealing, also indicating that annealing may affect the conduction mechanism. It is observed that κ of decreasing temperature measurements for the first anneal after exposure to atmosphere is lower than decreasing temperature measurements for subsequent anneals (without further exposure). This is consistent with previous results. However, no conclusions can be made at this time.

Acknowledgements

I would like to thank my advisor, Prof. James Kakalios, for giving me the opportunity to work with him, and for his willingness to take on a new project with me despite my short time in his lab. In addition to guiding me through this work, he also gave me invaluable career and research advice, giving me new insight into how experiments are conducted in physics with humor and positivity.

Additionally, I would like to thank Zvie Razieli, who grew my sample and taught me how to operate the equipment in the lab, as well as fixing and troubleshooting the equipment so many times. I would like to thank Brendon Jones and Jake Novotny for providing data and figures, as well as introducing me to the measurement process. I would also like to thank Paul Friedrichsen for carrying out simulations relating to the Zabrodskii analysis.

I would also like to thank Prof. Jochen Mueller and Prof. Rafael Fernandes for agreeing to be my thesis readers, and for taking the time out of their busy schedules to help me. I would like to thank Prof. Paul Crowell, for his guidance through the thesis project process and for his advice on presentations.

References

[1] Pereira, R. N., D. J. Rowe, R. J. Anthony, and U. Kortshagen. "Freestanding Silicon Nanocrystals with Extremely Low Defect Content." Phys. Rev. B Physical Review B 86.8 (2012).

[2] Holman, C. Z., C. Liu, and U. R. Kortshagen. "Germanium and Silicon Nanocrystal Thin-Film Field-Effect Transistors from Solution." Nano Lett. 10 (2010).

[3] Wienkes, L. R., C. Blackwell, and J. Kakalios. "Electronic Transport in Doped Mixed-phase Hydrogenated Amorphous/nanocrystalline Silicon Thin Films." Appl. Phys. Lett. Applied Physics Letters 100.7 (2012).

[4] Jones, Brendon. "Conductivity in Nanocrystalline Silicon Films." University of Minnesota Undergraduate Honors Thesis (2016).

[5] L. Mangolini, E. Thimsen, and U. Kortshagen, Nano Lett. 5, 655 (2005).

[6] L. R. Wienkes, C. Blackwell, and J. Kakalios, in Amorphous and Polycrystalline Thin-Film Silicon Science and Technology, edited by B. Yan, S. Higashi, C. C. Tsai, Q. Wang, and H. Gleskova (Mater. Res. Soc. Symp. Proc. 1321, Pittsburgh, PA, 2011), p. 285.

[7] Wienkes, Lee Raymond. "Electronic transport in mixed-phase hydrogenated amorphous/nanocrystalline silicon thin films." University of Minnesota Ph.D. Thesis (2013).

[8] Bodurtha, K., and J. Kakalios. "Non-Arrhenius Anomalous Hopping Electronic Transport in Hydrogenated Amorphous Silicon and Composite Amorphous/nanocrystalline Thin Films." J. Appl. Phys. Journal of Applied Physics 118.21 (2015).